Millijoule pulse energy 100-nanosecond Er-doped fiber laser

Leonid Kotov,[1,2,3,*] Mikhail Likhachev,[1] Mikhail Bubnov,[1] Oleg Medvedkov,[1] Denis Lipatov,[4,5] Aleksei Guryanov,[4] Kirill Zaytsev,[3] Mathieu Jossent,[3] and Sébastien Février[3]

[1]*Fiber Optics Research Center of the Russian Academy of Sciences, 38 Vavilov Street, Moscow 119333, Russia*

[2]*Moscow Institute of Physics and Technology, 9 Institutskii per., Dolgoprudny, Moscow Region 141700, Russia*

[3]*XLIM, UMR 7252 CNRS - University of Limoges, 123 Avenue Albert Thomas, 87060 Limoges, France*

[4]*Institute of Chemistry of High Purity Substances of the Russian Academy of Sciences, 49 Tropinin Street, Nizhny Novgorod 603950, Russia*

[5]*Lobachevsky State University of Nizhnii Novgorod, 23 Prospekt Gagarina, Nizhnii Novgorod 603950, Russia*

**Corresponding author: kotov@fo.gpi.ru*

Received December 4, 2014; revised February 12, 2015; accepted February 12, 2015;
posted February 18, 2015 (Doc. ID 229039); published March 17, 2015

We report, for the first time to our knowledge, on a single-mode millijoule-level 100-nanosecond Er-doped fiber laser operating near 1550 nm. The system features a newly developed 35-μm-core Yb-free double-clad Er-doped fiber based on P_2O_5-Al_2O_3-SiO_2 glass matrix and produces pulses with energy as high as 1 mJ at repetition rates of 1–10 kHz.

OCIS codes: (140.3510) Lasers, fiber; (060.2410) Fibers, erbium; (060.2320) Fiber optics amplifiers and oscillators; (140.3538) Lasers, pulsed.

http://dx.doi.org/10.1364/OL.40.001189

Pulsed fiber lasers operating near 1.55 μm are good candidates for many applications such as light detection and ranging (LIDAR) and atmospheric communication because of their relative eye-safety and high transparency of the atmosphere in this spectral range. High-energy (>1 mJ) extraction at 1.55 μm is usually based on the amplification of nanosecond-duration pulses using large-mode-area (LMA) Er-doped fiber amplifiers (EDFAs) [1–5]. However, until now, all demonstrated high-energy ns lasers at 1.55 μm suffer from poor beam quality ($M^2 > 1.5$) [1–5]. In this Letter, we demonstrate, for the first time to the best of our knowledge, a mJ-pulse energy single-mode nanosecond Er-doped fiber laser.

Power scaling with Er-doped fibers is highly challenging compared to Yb-doped fibers for example, because of the low absorption cross-section of Er^{3+} and decreasing efficiency at high erbium concentrations, which is caused by the clustering of Er^{3+} ions. These two factors impede simple realization of efficient cladding-pumped lasers and amplifiers.

Core pumping with a high power Raman laser appears promising to reduce Er-doped fiber nonlinearity [5]. However, the scheme becomes cumbersome, because it consists of an Yb-doped fiber laser at 1064 or 1117 nm, five or six cascaded Raman laser, and an Er-doped fiber amplifier. Second, and more crucial, this approach requires high-power 1480/1550-nm wavelength division multiplexers, which are available as experimental samples only and are subject to rapid power degradation [6].

At the moment, Er-Yb co-doped fibers that are cladding pumped in the Yb absorption band are used successfully to obtain high average power at 1.55 μm. A weakness of these fibers is a high core refractive index (because of the P_2O_5 high doping level required for efficient energy transfer from Yb^{3+} to Er^{3+} ions), which limits the single-mode core diameter to less than 10 μm and does not allow the reduction of fiber nonlinearity. Another drawback is the appearance of amplified spontaneous emission (ASE) from Yb^{3+} ions near 1 μm for output power higher than 10 W [7], which alters the slope efficiency and compromises the laser eye-safety. These problems make Er-Yb fibers unsuitable for pulsed lasers with high peak powers. Thus, to date, the highest pulse energy obtained using such an approach is restricted to 0.2 mJ for phosphate [8] and 0.1 mJ for silica-based fibers [9].

For Yb-free Er-doped fibers, the best results in terms of pump conversion efficiency (PCE) and average power scaling were obtained using resonant-pumping schemes at 1532 nm because of the low quantum defect [3,10]. This approach was used to reach the mJ energy level for 180 ns pulses near 1.5 μm with an M^2 of 1.6 [3]. However, sources for in-band pumping are much less competitive than diode pumping at 976 nm in terms of both cost and wall-plug efficiency.

Record wall-plug efficiency for continuous-wave (CW) fiber sources of multiple tens of Watts near 1.55 μm was recently demonstrated by our group using a laser based on the newly developed Yb-free large-mode-area Er-doped fiber and cladding pumping at 976 nm [11]. The fiber has a SiO_2-Al_2O_3-F core with a diameter of 35 μm. Fluorine co-doping was used in this case to decrease the core/cladding refractive index difference to $\Delta n \sim 0.0012$, ensuring effective single transverse mode propagation at the laser wavelength. However, the proposed design is not suitable for high-energy ns pulse amplification because of a low erbium concentration, which results in a long amplifier length (~45 m). The dependence of PCE on the Er^{3+} concentration was calculated in [11] for such fiber amplifier operated at 1585 nm, and is presented again in Fig. 1 (dashed line). Increasing the erbium concentration leads to a decrease of the fiber length and reduces the nonlinearity. However, it also reduces PCE because the number of Er^{3+} clusters increases significantly. We have shown [12] that the erbium cluster solubility can be improved for low-NA Er-doped

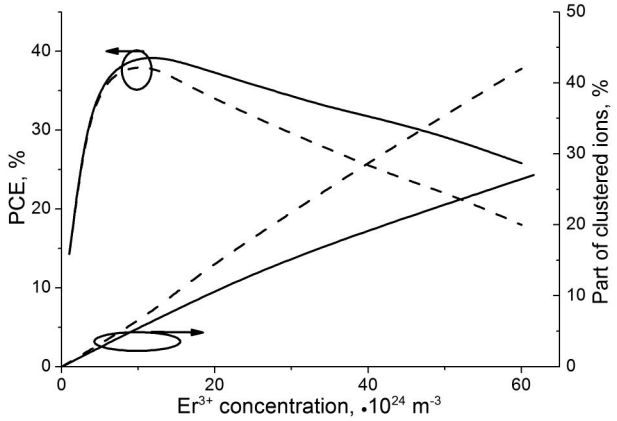

Fig. 1. Calculated PCE and part of the clustered ions versus the Er^{3+} concentration for fibers based on Al_2O_3-SiO_2-F (dashed) and P_2O_5-Al_2O_3-SiO_2 (solid) 35/125 fibers.

fibers using a P_2O_5-Al_2O_3-SiO_2 (PAS) glass matrix as the host for Er^{3+} ions. Using the technique described in Ref. [10], we calculated the dependence of the number of clusters on the erbium concentration in PAS glass matrix. We used the pair-induced quenching model that considers only the existence of clusters with two ions. Using these data, the PCE for 35/125-μm fibers operating at 1585 nm was also computed. The results of this computation for PAS glass are also shown in Fig. 1 with solid curve. As observed, the number of Er ion clusters increases much more slowly with the concentration for PAS glass. Thus, a significantly higher PCE at high erbium concentrations can be obtained with this new glass matrix.

Using a modified chemical vapor deposition technique, we elaborated a highly Er-doped preform, from which we drew down a double-clad fiber. Core compound was based on the PAS glass matrix and doped with ~0.1 mol.% Er_2O_3 ($\sim 50 \cdot 10^{24}$ m^{-3}). The fiber core diameter is 35 μm. The refractive index profile (RIP), calculated fundamental mode field distribution, fiber facet image, and near-field intensity pattern, which was recorded at the output of the fiber operated in the CW power amplifier regime, are shown in Fig. 2. The

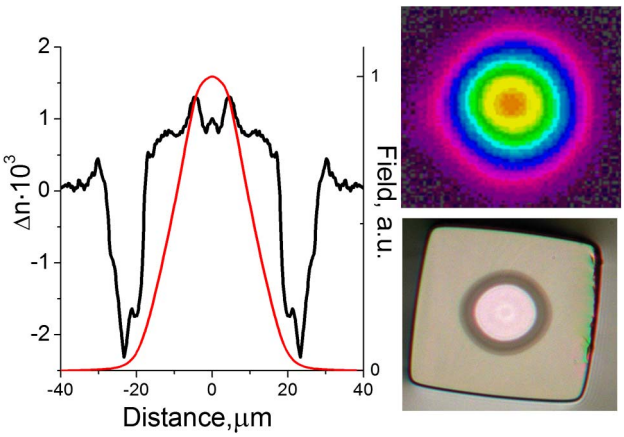

Fig. 2. Refractive index profile, calculated fundamental mode field distribution, optical image of the fiber end facet, and near-field intensity pattern recorded in the high-power CW regime.

calculated mode field diameter (MFD) at $1/e^2$ in intensity is 24.7 μm at 1550 nm. LP11 mode cut-off wavelength was measured in the unpumped fiber to be about 1650 nm. This experimental result was confirmed by computing the spectral variation of the propagation constant of the LP11 mode taking into account the measured refractive index profile shown in Fig. 2. The effective single-mode operation regime was also checked by measuring a gain spectrum of the LMA EDFA with a superluminescent wideband (~30 nm) source as a signal. The presence of a LP11 mode in this case could be estimated from the amplitude of periodical modulation of the gain spectrum that corresponds to the interference between two guided modes. Our estimation shows that a part of the high-order mode is less than a few percent, i.e., below the accuracy of this method. The fiber cladding has a square shape with a surface area of 110 μm × 110 μm, which is equivalent to that of a circular fiber with a diameter of 125 μm. The fiber was coated with a low-index polymer that provides NA of 0.46. As a result, the pump radiation from a standard pump combiner can be coupled into the double-clad active fiber with negligible loss. The measured small-signal absorption from the cladding was equal to 3 dB/m at 980 nm.

The scheme of the all-fiber master oscillator power amplifier (MOPA) laser used in this work is shown in Fig. 3. We started from a CW erbium-doped fiber laser (EDFL). The cavity of this laser was formed using a pair of fiber Bragg gratings at 1560 nm with bandwidth of 0.5 nm and a telecom erbium-doped fiber. The laser was core-pumped at 980 nm using a single-mode diode (SMD) with an output power of 400 mW. Then the radiation from this laser was modulated using an acousto-optical modulator (AOM) with ~100 ns pulse duration. The pulse repetition rate could be varied from 1 to 10 kHz during the experiments. The pulse train was pre-amplified in a telecom-grade EDFA to pulse energy of ~10 μJ. A fiber circulator and a high-reflective (>99%) fiber-Bragg grating (HR FBG) were used to clean the signal spectrum from out-of-band ASE. The reflection spectrum of this grating was matched to that of the FBGs in the EDFL. Then, we used 5.5 m of ytterbium-free double-clad LMA EDF to boost a signal. To ensure effective single-mode operation, the fiber was gently bent (bend diameter ~30 cm) during the amplification experiments. The LMA EDF was cladding pumped using multimode diodes (MMD) at 976 nm with maximum available power of 100 W. The pump and signal were launched into the active fiber through a commercially available pump combiner with 20/125 μm core/cladding diameters (NA ~ 0.08/0.46) signal ports to provide a robust all-fiber construction of the laser scheme. A cladding light stripper (CLS) was fabricated near the end of the Er-doped fiber to eliminate any unabsorbed pump power and potential cladding signal

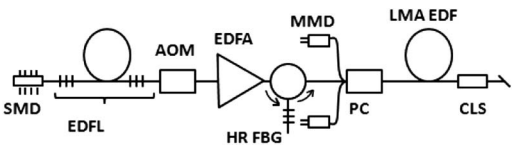

Fig. 3. Sketch of the all-fiber nanosecond MOPA system.

modes. An angle-cleaved end of the active fiber was used as the output coupler.

In order to accurately measure the actual extracted energy and to assess the performance of an EDFA, one must measure fraction of output power contained in the ASE. The ASE power cannot be detected by a standard photo-detector because of its limited power dynamics. To date, pyro-electric energy-meters that are insensitive to CW are often used to measure the pulse energy of nanosecond lasers. However, time-dependent ASE power can add to the pulse power and yield overestimated pulse energy. Gating of ASE in the time domain was recently used to characterize the fiber laser output in terms of ASE content [9]; this approach yields accurate measure pulse energy but requires additional equipment unavailable in our laboratory. In the present work, we used another approach based on an integrating photodetector scheme.

The circuitry of the detector in our experiment is shown in Fig. 4 and consists of a 1-GHz photodetector, a capacitor, and a low-noise, fast operational amplifier. The voltage at the capacitor reflects the total optical power integrating over time:

$$U(t) = C \cdot q(t) = \int_0^t C \cdot I(\tau) \cdot \mathrm{d}\tau = C \cdot S \cdot \int_0^t P(\tau) \cdot \mathrm{d}\tau, \tag{1}$$

where C is the capacitance of the capacitor, q is the charge accumulated in the capacitor, I is the current generated by the photodetector, S is the photodetector sensitivity, and P is the optical power received at the photodetector. The output of the operational amplifier reproduces the capacitor voltage without disturbing the photodetector-capacitor circuitry. Thus, the output voltage is proportional to the total optical energy received at the photo-detector from the beginning (when the capacitor is discharged) to time t. It must be noted that this scheme generates a signal that monotonically grows, and when the capacitor voltage exceeds the power supply voltage the scheme will not operate properly. Thus to ensure the desired operation regime of the capacitor, we equipped the scheme with a pulse counter, which discharge the capacitor after every eight pulses.

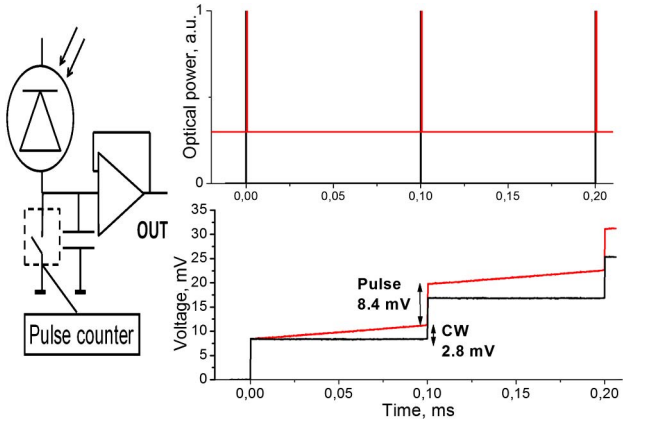

Fig. 4. Principal scheme of the integrating setup for ASE measurements (left part). Optical power temporal profile (top) and measured oscilloscope traces from integrating scheme (bottom) for a pulsed laser only (black) and a CW and pulsed laser (red).

To prove that this setup can measure the power accumulation in the time domain, we tested it using simultaneous CW and pulsed excitation. We combined the radiation of CW EDFL and 10-kHz 100-ns laser at 1560 nm through a 50/50 single-mode fiber coupler. The average power at the coupler output was set to 1 mW from the CW source and 3 mW from the pulsed one. Top graph in Fig. 4 is a schematic representation of the optical power coming to the photodetector for a pulsed laser with (red) and without (black) CW background. Bottom graph of Fig. 4 shows the corresponding trace recorded with an oscilloscope at the output of our integrating system. Recall that upper traces cannot be measured accurately due to saturation of the photodetector and are guides for the eye for further understanding of bottom traces. Let us consider the black trace first. At time $t < 0$, the capacitor is short-circuited, and at $t = 0$, this short-circuit is switched off. The sharp steps at $t = 0$ and $t = 0.1$ ms correspond to incoming nanosecond pulses, which quickly charge the capacitor. These steps have 100-ns duration that corresponds to the duration of the incoming 100-ns pulses. It is worth noting that the signal on capacitor does not change between pulses. This behavior demonstrates the absence of any optical power in between pulses. On the contrary, when the CW laser is on (red trace), the signal linearly increases due to integration of its power. As observed in Fig. 4, the signal accumulated in one duty cycle for pulsed radiation is 3 times higher than that for CW. This ratio perfectly matches the actual power ratio set at the beginning of the experiment. We performed this experiment for various power ratios, and the agreement was observed at all times. Thus, the integrating scheme allows us to measure a power contained in ASE at the output of the nanosecond laser. In the following, we define the actual pulse energy from this value, the average power and the repetition rate.

Using the aforementioned technique, we characterized the all-fiber MOPA. Figure 5 shows the measured dependence of the pulse energy on the launched pump power for various repetition rates. It also shows part of ASE at MOPA output at 10 kHz.

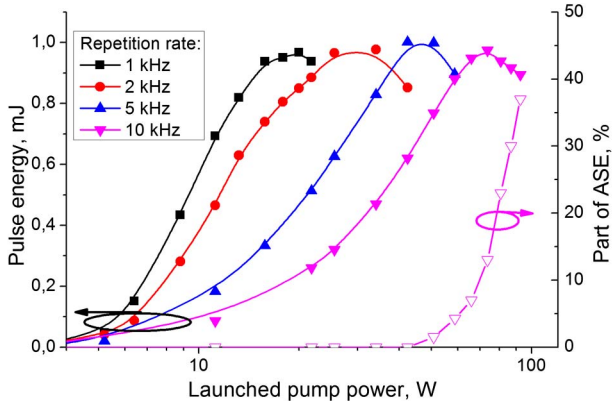

Fig. 5. Measured pulse energy for different repetition rates and part of ASE at the laser output at 10 kHz.

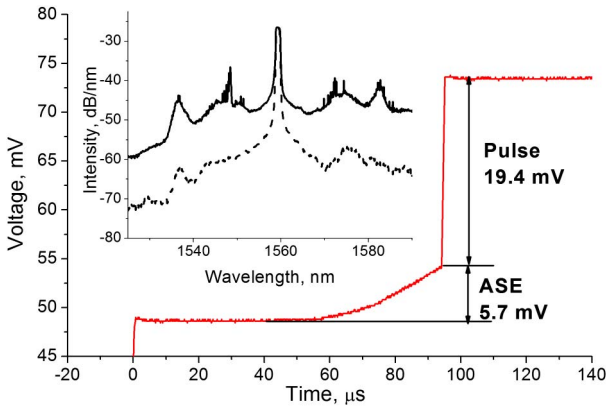

Fig. 6. Oscilloscope trace measured with the integrating scheme at 80.8-W pump power. Inset: output spectrum for 80.8-W (solid) and 65-W (dashed) W of pump power.

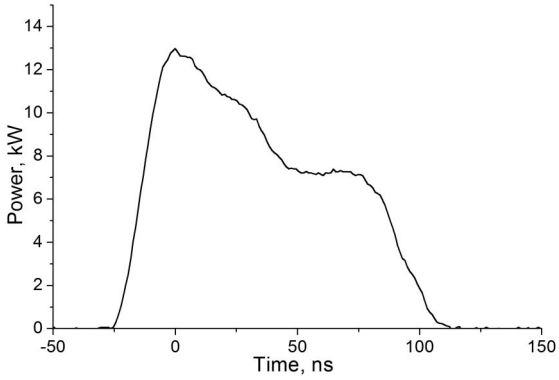

Fig. 7. Power temporal profile.

As observed in Fig. 5, the highest pulse energy was ~1 mJ, which does not depend on the repetition rate in the range of 1–10 kHz. It should be noted that for every repetition rate, the pulse energy saturates when the ASE part at the output reaches ~10%. Nevertheless, to the best of our knowledge, the attained energy of 1 mJ is one order of magnitude higher than the previous record for all-fiber silica-based single-mode nanosecond lasers near 1.5 μm [9]. The ASE dynamics that was measured using the integrating photodetector scheme at the pump power of 80.8 W and pulse repetition rate of 10 kHz is shown in Fig. 6. An ASE part at the laser output is 23% in this case. Optical spectrum at this pump power is presented as the inset in Fig. 6. Spectrum at lower pump power but at the same pulse energy is also presented in Fig. 6 (dashed).

The pulse power temporal profile at 1 mJ of pulse energy is presented in Fig. 7. The peak power reaches 13 kW. Because of depletion of inversion by a leading edge of the 100-ns pulse, the gain available for the trailing edge of the pulse is lower, which changes the amplified pulse shape. This behavior is typical for a long nanosecond MOPA system without pulse pre-shaping [13].

In conclusion, we have reported on the first demonstration of single-mode 100-ns nanosecond pulse amplification at 1560 nm to energy as high as 1 mJ. The power amplifier features a newly developed double-clad Er-doped Yb-free fiber with an MFD of 24.7 μm and a relatively high Er^{3+} concentration. Usage of the integrating photodetector scheme allowed us to accurately measure the ASE content. It was shown that the obtained energy was limited by the generation of ASE in the amplifier and did not depend on the pulse repetition rate.

This work was supported in part by the Russian Foundation for Basic Research (RFBR), grant 12-08-33101 and the French Agence Nationale de la Recherche under grant UBRIS2. Leonid Kotov acknowledges financial support from the French ministère des Affaires étrangères. The authors are grateful to I. A. Bufetov from Fiber Optics Research Center for fruitful discussion and E. M. Dianov, director of the Fiber Optics Research Center, for his continuous interest in and support of this work.

References

1. V. S. Desmoulins and F. Di Teodoro, Opt. Express **16**, 2431 (2008).
2. E. Lallier and D. Papillon-Ruggeri, *CLEO/Europe 2011* (Optical Society of America, 2011), paper CJ1.5.
3. E.-L. Lim, S. Alam, and D. J. Richardson, Opt. Express **20**, 18803 (2012).
4. V. Khitrov, V. V. Shkunov, D. A. Rockwell, Yu. A. Zakharenkov, and F. Strohkendl, Opt. Lett. **37**, 3963 (2012).
5. J. W. Nicholson, J. M. Fini, A. M. DeSantolo, X. Liu, K. Feder, P. S. Westbrook, V. R. Supradeepa, E. Monberg, F. DiMarcello, R. Ortiz, C. Headley, and D. J. DiGiovanni, Opt. Express **20**, 24575 (2012).
6. X. Peng, K. Kim, X. Gu, M. Mielke, S. Jennings, A. Rider, N. Fisher, T. Woodbridge, R. Dionne, and F. Trepanier, Opt. Express **21**, 20052 (2013).
7. E. Yahel and A. Hardy, J. Lightwave Technol. **21**, 2044 (2003).
8. W. Shi, N. Moor, R. Zhou, K. Al Yahyaei, D. T. Nguyen, Z. Yao, M. A. Stephen, A. Chavez-Pirson, and N. Peyghambarian, in *CLRC XVI Proceedings* (Universities Space Research Association, 2011), p. 129.
9. I. Pavlov, E. Dülgergil, E. Ilbey, and F. Ö. Ilday, Opt. Lett. **39**, 2695 (2014).
10. M. A. Jebali, J.-N. Maran, and S. LaRochelle, Opt. Lett. **39**, 3974 (2014).
11. L. V. Kotov, M. E. Likhachev, M. M. Bubnov, O. I. Medvedkov, M. V. Yashkov, A. N. Guryanov, J. Lhermite, S. Février, and E. Cormier, Opt. Lett. **38**, 2230 (2013).
12. M. E. Likhachev, M. M. Bubnov, K. V. Zotov, D. S. Lipatov, M. V. Yashkov, and A. N. Guryanov, Opt. Lett. **34**, 3355 (2009).
13. L. V. Kotov, M. E. Likhachev, M. M. Bubnov, V. M. Paramonov, M. I. Belovolov, D. S. Lipatov, and A. N. Guryanov, Laser Phys. Lett. **11**, 095102 (2014).